ELSEVIER

Journal of Power Sources 104 (2002) 248–252

JOURNAL OF POWER SOURCES

www.elsevier.com/locate/jpowsour

Thermal simulation of large-scale lithium secondary batteries using a graphite–coke hybrid carbon negative electrode and $LiNi_{0.7}Co_{0.3}O_2$ positive electrode

Atsuhiro Funahashi*, Yoshinori Kida, Katsunori Yanagida, Toshiyuki Nohma, Ikuo Yonezu

New Materials Research Center, SANYO Electric Co., Ltd., 1-1 Dainichi-higashimachi, Moriguchi, Osaka 570-8502, Japan

Received 16 February 2001; received in revised form 5 September 2001; accepted 25 September 2001

Abstract

Thermal simulation was applied to 2 Wh-class cells (diameter 14.2 mm, height 50 mm) using $LiNi_{0.7}Co_{0.3}O_2$ or $LiCoO_2$ as the positive electrode material, in order to clarify the thermal behavior of the cells during charge and discharge. The thermal simulation results for the 2 Wh-class cells showed a good agreement with measured temperature values. The heat generation of a cell using $LiNi_{0.7}Co_{0.3}O_2$ was found to be much less than that using $LiCoO_2$ during discharge. This difference was considered to be caused by the difference in the change of entropy. A 250 Wh-class cell (diameter 64 mm, height 296 mm) was also constructed using $LiNi_{0.7}Co_{0.3}O_2$ and thermal simulation was applied. We confirmed that the results of the thermal simulation agreed with measured values and that this simulation model is effective for analyzing the thermal behavior of large-scale lithium secondary batteries.

Keywords: Lithium secondary batteries; Thermal simulation; Graphite–coke hybrid; Carbon; $LiNi_{0.7}Co_{0.3}O_2$

1. Introduction

Recently, intensive efforts have been made to decrease the consumption of energy in Japan, in response to a growing difference in the electric power demand during the daytime and at night. To decrease the consumption of energy, one approach is to develop systems of efficient energy utilization by load leveling. The efforts of load leveling have mostly been on the supply side with pumped storage hydropower generation, and so on. However, taking into account the drastic increases in power demand in urban areas, further efforts concerning load leveling are now required on the demand side by, e.g. using dispersed type battery energy storage systems for home use. These batteries for load leveling systems must be designed to provide a long cycle life, such as 10 years.

Lithium secondary batteries using a carbon negative electrode have a high energy density and show an especially superior charge/discharge cycle performance. This is because, in their charge and discharge reactions, lithium ions transfer between the positive and negative electrodes and there are no significant changes in the crystal structures of both electrodes. Accordingly, lithium secondary batteries using a carbon negative electrode are an attractive candidate for dispersed type battery energy storage systems. From studies on various carbon materials as the negative electrode, we have found that graphite–coke hybrid carbon is a promising material as the negative electrode material for battery energy storage systems because of its excellent cycle performance and large discharge capacity [1].

On the other hand, in the development of lithium secondary batteries for energy storage systems, the thermal management of the cells is very important. This is because these batteries are required to have a much larger capacity than ordinary consumer batteries and because their charge/discharge currents become high. A number of studies involving thermal simulation have been made on lithium secondary batteries [2–11], in order to estimate the temperature changes during charge and discharge. Few studies, however, have confirmed a calculated temperature with a measured value by using actual large-scale cells.

In this study, the thermal simulation of large-scale lithium secondary batteries was investigated and the simulated values were confirmed by using 250 Wh-class cells. The thermal and electrochemical characteristics of different types of positive electrode materials (i.e. $LiCoO_2$ and $LiNi_{0.7}Co_{0.3}O_2$) were also examined to clarify the relationship between the thermal behavior and the entropy change.

* Corresponding author. Tel.: +81-6-6900-3556.
E-mail address: a_funahashi@rd.sanyo.co.jp (A. Funahashi).

0378-7753/02/$ – see front matter
PII: S0378-7753(01)00958-2

Nomenclature

c_p	specific heat capacity (J g^{-1} K^{-1})
E_0	electromotive force (V)
I_t	current (A)
Q	heat generation in the cell (J)
r	cell radius (mm)
t	time (s)
T	temperature (K)
V_t	cell voltage (V)
z	distance in the axis direction (mm)
Greek letters	
λ	thermal conductivity (W m^{-1} K^{-1})
ρ	density (g cm^{-3})

2. Experimental

2.1. 2 Wh-class cells

The diameter and height of each 2 Wh-class cylindrical cell were 14.2 and 50 mm. $LiCoO_2$ or $LiNi_{0.7}Co_{0.3}O_2$ was used as the positive electrode material and graphite–coke hybrid carbon was used as the negative electrode material. The graphite–coke hybrid carbon was prepared by mixing graphite and coke in a 4 to 1 weight ratio. A mixed solvent of ethylene carbonate and diethyl carbonate containing 1 M $LiPF_6$ was used as the electrolyte. A stainless steel vessel was used for the cells. The cells were charged with a constant current of 65 mA until the cell voltage reached 4.1 V and discharged with a constant current of 500 mA until the cell voltage reached 2.7 V.

2.2. 250 Wh-class cells

The diameter and height of each 250 Wh-class cylindrical cell were 64 and 296 mm. $LiNi_{0.7}Co_{0.3}O_2$ was used as the positive electrode material and the other materials were the same as those used for the 2 Wh-class cells. The cells were charged with a constant current of 8.8 A until the cell voltage reached 4.2 V and discharged with a constant current of 70 A until the cell voltage reached 2.7 V.

3. Model and assumptions of the thermal simulation

For the thermal simulation, we followed Kanari's method and the calculations for the cells were done with $LiCoO_2$ as reported by Kanari et al. [13]. A simplified model was also used under the following assumptions [2,12,13]:

1. A group in the cell rolls with both electrodes and the separator soaked in the electrolyte is made of a homogeneous material having effective thermophysical properties.
2. The heat generation is uniform in the cell during charge and discharge.
3. The convection and radiation heat transfer in the cell are neglected.
4. The temperature dependence of the thermophysical properties excluding the specific heat capacity of the separator is neglected.

Under the above assumptions, the following heat balance equation can be written for each part of the equipment.

$$c_p\rho\frac{\partial T}{\partial t} = \lambda_r\left(\frac{\partial^2 T}{\partial r^2} + \frac{1}{r}\frac{\partial T}{\partial r}\right) + \lambda_z\frac{\partial^2 T}{\partial z^2} + Q \quad (1)$$

where c_p is the specific heat capacity, ρ the density, λ the thermal conductivity, t the time, T the temperature, r the radius, z the distance in the axis direction, and Q is the heat generation in the cell.

All calculations were made with explicit finite difference equations and reported thermophysical properties [2,13] for the materials in the equipment. The heat generation in the cell was calculated by the following equations [2,12,13]:

$$Q_{\text{tot}} = Q_{\text{ent}} + Q_{\text{ohm}} \quad (2)$$

$$Q_{\text{ohm}} = (V_t - E_0) \times I_t \quad (3)$$

$$Q_{\text{ent}} = T\left(\frac{\mathrm{d}E_0}{\mathrm{d}T}\right) \times I_t \quad (4)$$

where Q_{tot} is the total heat generation, Q_{ent} the heat generation due to the change in entropy along with the electrochemical reactions on both electrodes, Q_{ohm} the heat generation due to the polarization including the ohmic voltage drop, V_t the cell voltage, I_t the current, and E_0 is the electromotive force. In Eq. (2), we neglect the heat generation due to the self-discharge of the cell and the side reaction in the cell.

In this study, the open circuit voltage was used instead of the electromotive force. In Eq. (3), the internal cell resistance is treated as a constant during charge/discharge. The value of ($\mathrm{d}E_0/\mathrm{d}T$) is calculated by approximate equations obtained from the experimental results shown in Fig. 5.

The positive electrode material was composed of 90 wt.% $LiNi_{0.7}Co_{0.3}O_2$, 5 wt.% polyvinylidene fluoride (PVdF), and 5 wt.% carbon. The negative electrode material was composed of 76 wt.% graphite, 19 wt.% coke, and 5 wt.% PVdF.

Cell parameters and their values for the thermal simulation of 2 Wh-class cells are listed in Table 1. The heat

Table 1
Simulation parameters and their values for 2 Wh-class cells

Cell parameters	Values
Diameter (mm)	14.2
Height (mm)	50
Initial temperature (K)	298
Environment temperature (K)	298
Heat transfer coefficient (W m^{-2} K^{-1})	10

transfer coefficient for the 2 Wh-class cells was the measured value. The model of the cells was divided at intervals of 1 mm in the r and z directions. The internal cell resistance of each 2 Wh-class cell was 200 mΩ, calculated from the current–voltage characteristics at the temperature of 298 K. The initial state of the experimental and thermal simulation in discharge was 0% for the depth of discharge maintained at 298 K after the rated capacity was charged at a C/8-rate.

4. Results and discussion

First, we measured the discharge characteristics of the 2 Wh-class cells in which $LiCoO_2$ or $LiNi_{0.7}Co_{0.3}O_2$ was used as the positive electrode material. The discharge curves of the 2 Wh-class cells are shown in Fig. 1. The cell using $LiNi_{0.7}Co_{0.3}O_2$ showed a larger discharge capacity of 0.5 than the 0.45 Ah displayed by the cell using $LiCoO_2$.

Next, the surface temperatures of these cells were measured during discharge. The surface temperatures of the 2 Wh-class cells during discharge are shown in Fig. 2. The discharge current was 500 mA, and this value nearly corresponded to the 1C-rate. Each discharge capacity at the 1C-rate of the 2 Wh-class cells was about 83% of the charge capacity. The surface temperature of the cell using $LiCoO_2$ increased to about 308 K from 298 K at the end of the discharge. The surface temperature of the cell using $LiNi_{0.7}Co_{0.3}O_2$ increased to about 301 K. The cell using $LiNi_{0.7}Co_{0.3}O_2$ showed a much lower surface temperature rise during the discharge than the cell using $LiCoO_2$. From these results, we found that the cells with different positive electrodes had different thermal behaviors. In particular, no significant temperature rise at the end region of the discharge was detected for the cell using $LiNi_{0.7}Co_{0.3}O_2$, but was seen for the cell using $LiCoO_2$.

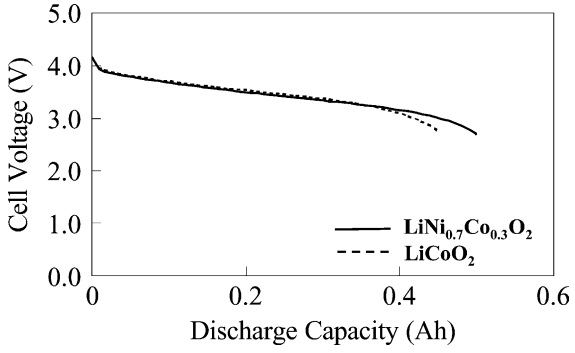

Fig. 1. Discharge curves of 2 Wh-class cells. Negative electrode: graphite–coke hybrid carbon; electrolyte: 1.0 mol l^{-1} $LiPF_6$–EC/DEC (1/1); charge current: 65 mA; discharge current: 500 mA.

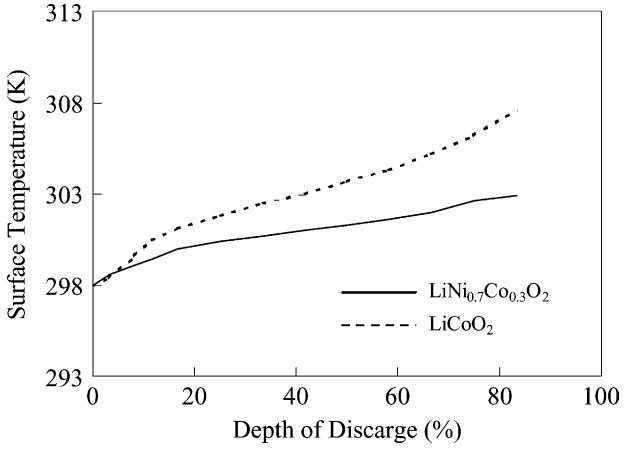

Fig. 2. Surface temperatures of 2 Wh-class cells during discharge. Discharge current: 500 mA.

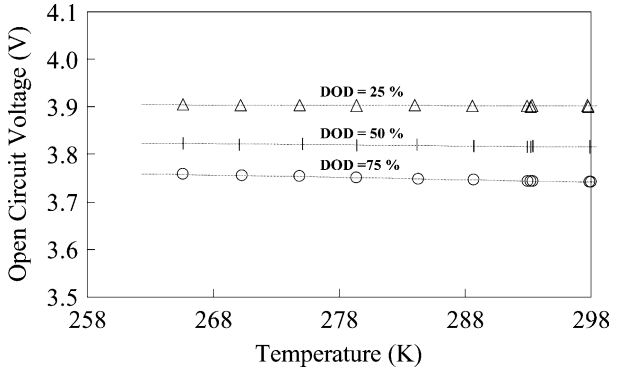

Fig. 3. Open circuit voltage vs. temperature of 2 Wh-class cells using $LiCoO_2$ measured at several depths of discharge.

Because the thermal behaviors of the 2 Wh-class cells above were quite different, we analyzed the thermal characteristics of these cells by thermal simulation. Fig. 3 shows the open circuit voltage versus temperature of the 2 Wh-class cell using $LiCoO_2$ measured at several depths of discharge. As the figure shows, the open circuit voltage slightly changes linearly according to the temperature, and the entropy change "ΔS" is calculated using the slope of the line. Fig. 4 is similar to Fig. 3 but with $LiNi_{0.7}Co_{0.3}O_2$ for the positive electrode.

From these results, the value of $(-dE/dT)$ was calculated for each cell, and plotted versus the depth of discharge in Fig. 5 [14]. The thermal characteristics were found to be quite different for the cells using different positive

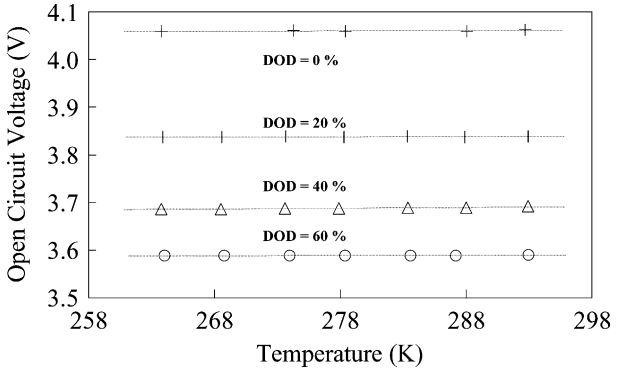

Fig. 4. Open circuit voltage vs. temperature of 2 Wh-class cells using $LiNi_{0.7}Co_{0.3}O_2$ measured at several depths of discharge.

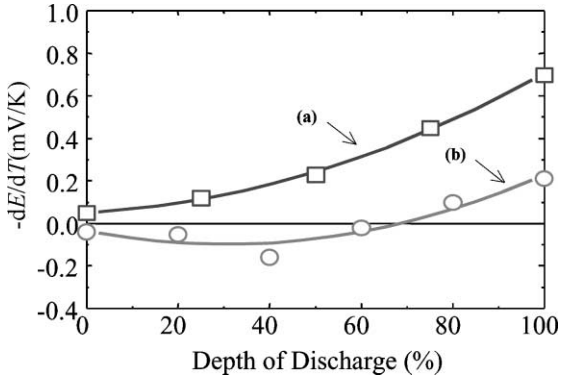

Fig. 5. Relationship between entropy change and depth of discharge (a) $LiNi_{0.7}Co_{0.3}O_2$, (b) $LiCoO_2$.

electrodes. In this figure, the upper area of the line, where the value of $(-dE/dT)$ is 0.0 mV, shows an exothermic reaction and the lower area shows an endothermic reaction during discharge. The cell using $LiCoO_2$ generated heat all the time during the discharge period. On the other hand, the thermal generation of the cell using $LiNi_{0.7}Co_{0.3}O_2$ changed according to the depth of discharge.

Following this, the data was put into the simulation equation and the temperature change for each cell during discharge was calculated. The results were compared with measured surface temperature values. Fig. 6 compares thermal simulation results and measured surface temperatures of 2 Wh-class cells during discharge. In this figure, the thermal

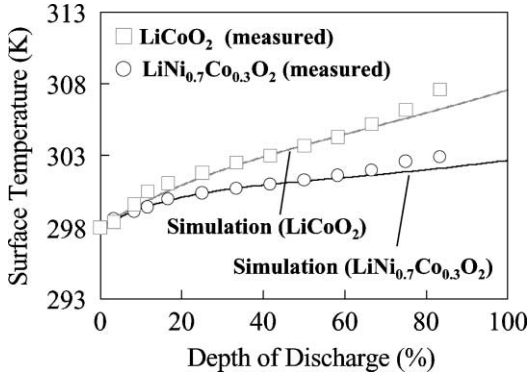

Fig. 6. Comparison of thermal simulation results and measured surface temperatures of 2 Wh-class cells during discharge.

Table 2
Specifications of a 250 Wh-class cell

Positive material	$LiNi_{0.7}Co_{0.3}O_2$
Negative material	Graphite–coke (4/1)
Electrolyte	$LiPF_6$–EC/DEC
Diameter (mm)	64.0
Length (mm)	296
Weight (kg)	2.2

Table 3
Simulation parameters and their values for a 250 Wh-class cell

Cell parameters	Values
Diameter (mm)	64.0
Height (mm)	296
Initial temperature (K)	298
Environment temperature (K)	298
Heat transfer coefficient (W m^{-2} K^{-1})	7

simulation results show a good agreement with the measured temperatures. In addition, it is clear that the cell using $LiNi_{0.7}Co_{0.3}O_2$ has a smaller heat generation than that using $LiCoO_2$.

Next, the thermal simulation model was applied to 250 Wh-class large cells. A 250 Wh-class cell is shown in Fig. 7 and the specifications of the 250 Wh-class cell are shown in Table 2. The cell parameters and their values are listed in Table 3. The heat transfer coefficient for the 250 Wh-class cells was the measured value. Like above, the model of the cells was divided at intervals of 1 mm in the r and z directions. The internal cell resistance of a 250 Wh-class cell was 8 mΩ, calculated from the current–voltage characteristics at the temperature of 298 K. $LiNi_{0.7}Co_{0.3}O_2$ was used for the positive electrode material, and the other materials were the same as those used for the 2 Wh-class cells except for an aluminum vessel. The change in voltage and the surface temperature were measured during the initial charge–discharge. The charge current was 8.8 A (which nearly corresponded to the C/8-rate) and the discharge current was 70 A (which nearly corresponded to the 1C-rate).

Fig. 8 shows the charge/discharge curves of a 250 Wh-class cell. The discharge capacity of this cell was about 97% of the charge capacity. Fig. 9 shows the surface temperature

Fig. 7. 250 Wh-class cell.

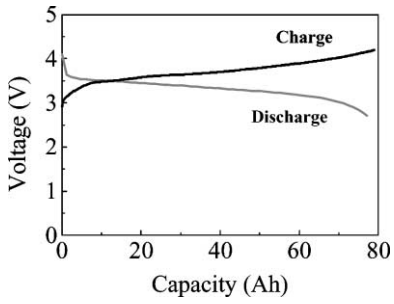

Fig. 8. Charge/discharge curves of a 250 Wh-class cell.

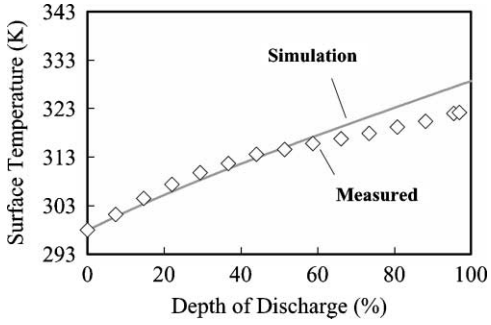

Fig. 9. Thermal simulation results and measured surface temperatures of a 250 Wh-class cell during discharge. Charge: *C*/8 (8.8 A); discharge: 1*C* (70 A).

of a 250 Wh-class cell measured during discharge and the thermal simulation results. The thermal simulation results closely match the actual measurements. But the measured surface temperature values in the latter half of the measurement period are lower than the thermal simulation values. We believe that this difference resulted from the decrease in the resistance of the cell by the heat generation. A future task will therefore, be to incorporate the dependence of the resistance on the temperature and depth of discharge into the thermal simulation.

5. Conclusions

The results in this paper are summarized as follows:

1. The thermal simulation results of a 2 Wh-class cell showed good agreement with measured temperature values.
2. The heat generation of a cell using $LiNi_{0.7}Co_{0.3}O_2$ was less than that using $LiCoO_2$ during discharge. This difference was caused by the difference in the change of entropy. $LiNi_{0.7}Co_{0.3}O_2$ was found to be a suitable positive electrode material for large-scale cells because of its small heat generation.
3. A 250 Wh-class cell using $LiNi_{0.7}Co_{0.3}O_2$ was constructed, and its simulation results were in accord with measured temperature values. The simulation was found to be efficient in estimating the thermal characteristics of both small-sized cells and large-scale cells.

Acknowledgements

We applied the original simulation program developed by the Electrotechnical Laboratory for this work. This work was performed as a part of the lithium secondary battery energy storage technology associate (LIBES) under contract for an R&D program of the New Energy and Industrial Technology Development Organization (NEDO).

References

[1] H. Kurokawa, T. Nohma, M. Fujimoto, T. Maeda, K. Nishio, T. Saito, Extended Abstract of the International Workshop on Advanced Batteries, Japan, 1995, p. 332.
[2] K. Kanari, T. Takano, Y. Saito, Bull. Electrotech. Lab. 60 (1996) 825.
[3] Y. Chen, J.W. Evans, J. Electrochem. Acta 39 (1994) 517.
[4] Y. Chen, J.W. Evans, J. Electrochem. Soc. 140 (1993) 1833.
[5] Y. Chen, J.W. Evans, J. Electrochem. Soc. 141 (1994) 2947.
[6] C.R. Pals, J. Newman, J. Electrochem. Soc. 142 (1995) 3274.
[7] C.R. Pals, J. Newman, J. Electrochem. Soc. 142 (1995) 3282.
[8] J. Kim, T.V. Nguyen, R.E. White, J. Electrochem. Soc. 139 (1992) 2781.
[9] K. Kanari, K. Takano, Y. Saito, T. Masuda, Extended Abstract of the International Workshop on Advanced Batteries, 1995, p. 278.
[10] Y. Saito, K. Kanari, K. Takano, J. Power Sources 68 (1997) 451.
[11] P. Flament, Ph. Jehanno, J.P. Planchat, G. Sarre, J.J. Vullierme, in: Proceedings of EVS-13, Vol. I, 1996, p. 632.
[12] K. Kanari, T. Takano, T. Masuda, R. Ishikawa, H. Shiota, T. Nohma, T. Ono, M. Terasaki, Bull. Electrotech. Lab. 60 (1996) 837.
[13] K. Kanari, Y. Saito, K. Harada, S. Yamanaka, Netsu Bussei 10 (2/3) (1996) 59.
[14] I. Yonezu, T. Maeda, Y. Chikano, K. Ohkita, H. Kurokawa, T. Nohma, K. Nishio, CD-ROM, in: Proceedings of the 15th International Electric Vehicle Symposium, 1998.